Inverse Faraday effect in graphene and Weyl semimetals

I. D. Tokman,[1,2] Qianfan Chen,[3] I. A. Shereshevsky,[1,2,4] V. I. Pozdnyakova,[1,2,4] Ivan Oladyshkin,[5] Mikhail Tokman,[5] and Alexey Belyanin[3]

[1]*Institute for Physics of Microstructures, Russian Academy of Sciences, Nizhny Novgorod 603950, Russia*
[2]*Lobachevsky State University of Nizhny Novgorod, Nizhny Novgorod 603950, Russia*
[3]*Department of Physics and Astronomy, Texas A&M University, College Station, Texas 77843, USA*
[4]*Sirius University of Science and Technology, 354340 Sochi, Russia*
[5]*Institute of Applied Physics, Russian Academy of Sciences, Nizhny Novgorod 603950, Russia*

(Received 8 March 2020; accepted 5 May 2020; published 19 May 2020)

We report systematic theoretical studies of the inverse Faraday effect in materials with massless Dirac fermions, both in two dimensions such as graphene and surface states in topological insulators, and in three dimensions such as Dirac and Weyl semimetals. Both semiclassical and quantum theories are presented, with dissipation and finite-size effects included. We find that the magnitude of the effect can be much stronger in Dirac materials as compared to conventional semiconductors. Analytic expressions for the optically induced magnetization in the low-temperature limit are obtained. Strong inverse Faraday effect in Dirac materials can be used for the optical control of magnetization, all-optical modulation, and optical isolation.

DOI: 10.1103/PhysRevB.101.174429

I. INTRODUCTION

Inverse Faraday effect (IFE) is a fascinating nonlinear optical phenomenon. Its key feature is generation of a permanent magnetization in a medium as a result of interaction with circularly polarized radiation [1]. The effect was predicted by Pitaevskii [2], and the name IFE was coined in [3–5]. IFE was studied extensively in plasmas, metals, and semiconductors [6–13]. More recent studies explored the use of IFE for ultrafast modulation of magnetization with femtosecond laser pulses [14–23] .

There has been a lot of recent interest in the optical properties of two- and three-dimensional (2D and 3D) materials with Dirac and Weyl fermions, including the nonlinear optical [24–38] and magneto-optical [39–44] response of graphene and Dirac/Weyl semimetals. Strong light-matter coupling in these systems makes them promising for IFE studies. In [24,45] the generation of edge photocurrent in graphene was studied theoretically and in experiments. We show below that generation of edge photocurrent is related to IFE.

In the Introduction we discuss general features of IFE based on the Pitaevskii formula (1) obtained from thermodynamic considerations. Section II develops a quasiclassical theory of IFE in graphene based on the kinetic equation. The quantum-mechanical derivation of IFE in graphene including interband transitions is given in Sec. III. Both Secs. II and III neglect dissipation. In Sec. IV we calculate the magnetization of graphene by directly summing over the magnetic moments of individual electrons (in quasiclassical approximation), instead of using the Pitaevskii formula. That is why we can include dissipation in this treatment. Section V takes into account finite-size effects and calculates edge photocurrent. Section VI develops the kinetic-equation theory for the IFE in Weyl semimetals. In Appendix A we evaluate the effect of the depolarization field on the IFE in a finite sample, whereas Appendix B studies saturation of IFE in strong fields. Throughout the paper, we include only the electric-dipole interaction with the electric field of the electromagnetic waves, ignoring a much smaller contribution of electron spins.

In a transparent nonmagnetic medium, i.e., in the medium with magnetic permeability $\mu = 1$, the magnetization excited by a monochromatic field can be determined from thermodynamic considerations. The resulting expression is [1]

$$\mathbf{m} = \sum_{ij} \frac{\partial \varepsilon_{ij}}{\partial \mathbf{H}} \frac{\widetilde{E}_j \widetilde{E}_i^*}{16\pi}, \tag{1}$$

where the optical field is given by $\mathbf{E} = \mathrm{Re}(\tilde{\mathbf{E}} e^{-i\omega t})$, i, j are Cartesian indices, ε_{ij} is a Hermitian tensor of the dielectric permittivity, $\mathbf{H}$ is the vector of a constant magnetic field. Here, the Gaussian units are assumed. In the absence of an external magnetic field, the derivative in Eq. (1) should be calculated in the limit $\lim_{\mathbf{H}\to 0}(\frac{\partial \varepsilon_{ij}}{\partial \mathbf{H}})$. If the medium is isotropic at $\mathbf{H} \to 0$ the induced magnetic moment will be orthogonal to the plane containing the electric field vector $\mathbf{E}$ (see Fig. 1). The magnitude of magnetization is determined by the difference between the intensities of right- and left-circularly polarized components of the optical field. It is obviously zero for a linearly polarized field.

It is remarkable that Eq. (1) remains valid for media with frequency dispersion: there is no need to add frequency derivatives $\frac{\partial \varepsilon_{ij}}{\partial \omega}$ to Eq. (1) whereas such derivatives are present in the expression for an averaged energy of the optical field in a dispersive medium [1,2]. The limit of zero dissipation is more subtle. As we show in Sec. IV in the quasiclassical approximation, Eq. (1) cannot be obtained by taking the real part of the complex dielectric function of the dissipative medium.

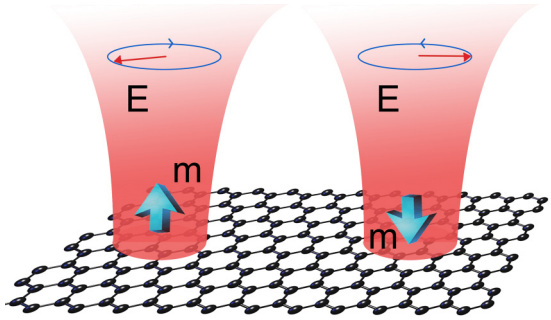

FIG. 1. A sketch of inverse Faraday effect: an incident circularly polarized light induces magnetization in a sample.

Equation (1) underscores another unique feature of the IFE. It is well known that any optical response that is quadratic in powers of the field can be calculated within a standard perturbative approach from the second-order (with respect to the field) perturbation of the density matrix. For a photoinduced magnetic moment in a system with discrete energy spectrum, such an approach was developed, e.g., in [46]. At the same time, Eq. (1) shows that it is possible to calculate photoinduced magnetization from the *linear* dielectric response of the medium.

It follows from Eq. (1) that IFE exists only in the media that become gyrotropic in an external constant magnetic field. Examples of the systems that *do not* become gyrotropic in an external magnetic field include an electron-positron plasma and magnetized vacuum [47]. Condensed matter systems with complete electron-hole symmetry are also not gyrotropic in an external magnetic field. One obvious example is a material with electronic band structure in the form of isotropic Dirac cones, when the Fermi level crosses the Dirac points, such as graphene or certain types of Dirac/Weyl semimetals [44]. Of course, this also implies low enough photon frequencies that probe only the range of electron energies close to the Dirac point. The selection rules for such systems allow one to group all electric-dipole allowed optical transitions into symmetric pairs $n \to -(n+1)$ and $n+1 \to -n$ with the same transition frequency but opposite direction of rotation of a circularly polarized optical field [44,48,49]. Gyrotropy, and therefore the IFE, will appear in these materials only when the Fermi level is shifted with respect to the Dirac/Weyl point; see Fig. 2. Moreover, as we argue below, the IFE is strongest in the limit of small frequencies and large Fermi energies, when resonant interband transitions are Pauli-blocked minimizing absorption and the main contribution to IFE comes from intraband transitions in the vicinity of the Fermi level.

Since the model leading to Eq. (1) does not include dissipation, for condensed matter systems it can give only a qualitative description. Nevertheless, it provides a useful limit based on general thermodynamic relations. In Sec. IV we compare it with a specific model that does take dissipation into account.

II. QUASICLASSICAL THEORY OF IFE IN GRAPHENE

For a 2D system such as graphene, it is convenient to use the electric susceptibility tensor instead of the dielectric

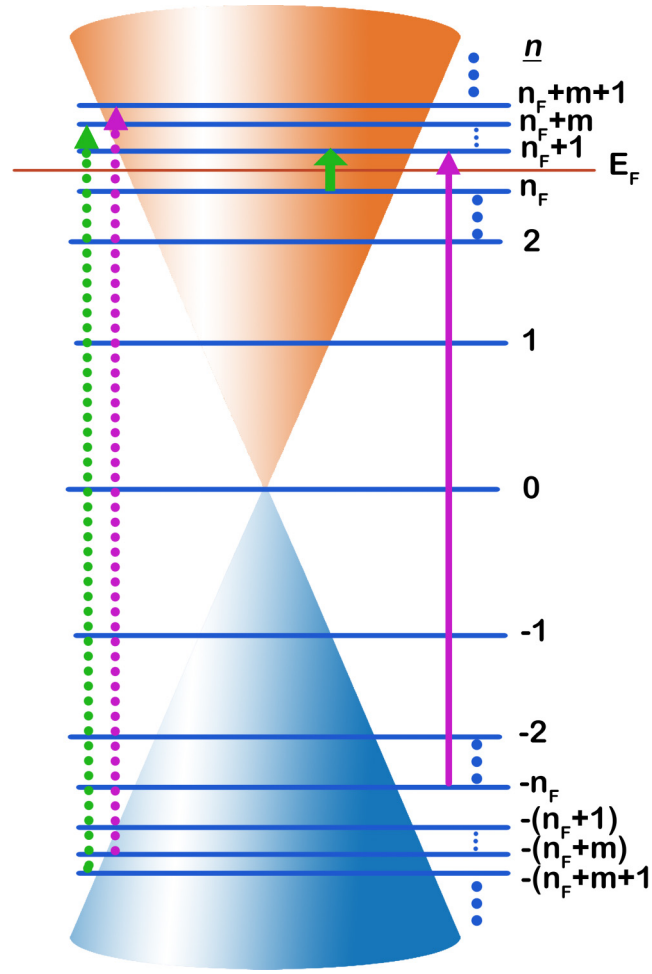

FIG. 2. Landau levels and optical transitions in graphene. The highest Landau level below the Fermi energy is denoted as n_F. Dotted arrows indicate a pair of transitions with contributions to the induced magnetic moment that cancel each other. Only the transitions shown with solid arrows (one interband and one intraband) contribute to inverse Faraday effect at low temperature.

permittivity in Eq. (1), namely, $\chi_{ij} = \frac{\varepsilon_{ij}-\delta_{ij}}{4\pi}$, and integrate this equation over the layer thickness. In this case, Eq. (1) becomes

$$\mathbf{m} = \sum_{ij} \frac{\partial \chi_{ij}}{\partial \mathbf{H}} \frac{\widetilde{E}_j \widetilde{E}_i^*}{4}. \tag{2}$$

Now the tensor χ_{ij} is a 2D surface susceptibility tensor which has the dimension of length; $i, j = x, y$ are coordinates in the graphene plane. The vector $\mathbf{m}$ in Eq. (2) has a meaning of a magnetic moment of a unit area (see Fig. 1). We will use a standard low-energy effective Hamiltonian for electrons near the Dirac point [50]:

$$\hat{H}_0 = v_F \hat{\mathbf{p}} \cdot \hat{\boldsymbol{\sigma}}, \tag{3}$$

where $\hat{\boldsymbol{\sigma}} = \mathbf{x}_0 \hat{\sigma}_x + \mathbf{y}_0 \hat{\sigma}_y$, $\hat{\mathbf{p}} = \mathbf{x}_0 \hat{p}_x + \mathbf{y}_0 \hat{p}_y$, $\hat{\sigma}_{x,y}$ are Pauli matrices, $\hat{p}_{x,y}$ are Cartesian components of the momentum operator, $\mathbf{x}_0$, $\mathbf{y}_0$ are unit vectors of coordinate axes, v_F is the Fermi velocity. In this model, the degeneracy factor $g = 4$ (two spin states and two valleys). The corresponding electron energies

are

$$W(p) = sv_F p, \tag{4}$$

where $p = \sqrt{p_x^2 + p_y^2}$; index $s = \pm 1$ corresponds to the conduction and valence band, respectively.

The analysis below is applicable also to 2D surface states in 3D topological insulators such as Bi_2Se_3. Their low-energy Hamiltonian is related to that of graphene by a unitary transformation, and the resulting linear and nonlinear optical responses are both very similar, after rescaling the values of the Fermi velocity and degeneracy (see, e.g., [29,31,42]).

Since in this model the IFE appears only when the Fermi energy is shifted from the Dirac point, we consider doped graphene and assume that the Fermi level is in the conduction band for definiteness. In the limit of small enough frequencies, low temperatures, and large Fermi energies (so that the contribution of interband transitions can be neglected) the quasiclassical theory is adequate. (This is the most interesting limit anyway: the results for a classical plasma, metals, and semiconductors [6–13] indicate that the photogenerated magnetic moment grows with decreasing frequency as $\propto\omega^{-3}$.) Indeed, it was shown in [31] that under rather weak restrictions on the nonuniformity of the electromagnetic field in the plane of graphene both linear and quadratic intraband susceptibilities derived within the quantum-mechanical density matrix formalism coincide with the results obtained from the kinetic equation based on the quasiclassical equations of motion for carriers. The nonuniformity restriction is $L \gg \frac{\hbar}{p_F}$, where L is the spatial scale of the nonuniformity of the field and p_F is the Fermi momentum related to the Fermi energy by $W_F = v_F p_F$. The contribution of interband transitions will be small when electrons are degenerate and

$$W_F \gg \hbar\omega. \tag{5}$$

This is confirmed by fully quantum treatment in Sec. III.

Under a more restrictive condition $L \gg \frac{v_F}{\omega}$ one can calculate the response neglecting spatial nonuniformity of the optical field [31]. We will use the kinetic equation which corresponds to the quasiclassical equations of motion [27,28,35,40,41]. To calculate the derivative in Eq. (2) it is enough to know the dependence of the tensor elements χ_{ij} on the external constant magnetic field in linear approximation with respect to $\mathbf{H}$. Here, the magnetic field is orthogonal to the monolayer: $\mathbf{H} = \mathbf{z}_0 H_z$. The kinetic equation has the form

$$\frac{\partial f}{\partial t} - e\left\{\mathbf{E}(t) + \left[\frac{1}{c}\left(\frac{\partial W}{p\partial p}\right)\mathbf{p} \times \mathbf{H}\right]\right\} \cdot \frac{\partial f}{\partial \mathbf{p}} = \hat{Q}(f). \tag{6}$$

Here, $\hat{Q}(f)$ is the relaxation operator, the electric field vector $\mathbf{E}$ is in the graphene plane, $-e$ is electron charge. We do not specify any particular electron dispersion $W(p)$ in Eq. (6) in order to compare the results for linear and quadratic dispersion (see also [13]).

Consider Eq. (6) when $\hat{Q}(f) = 0$. We need to calculate the linear response to the uniform high-frequency field $E_{x,y} = \mathrm{Re}(\tilde{E}_{x,y} e^{-i\omega t})$. We will seek the solution to Eq. (6) in the form $f = \mathrm{Re}[\delta f(\theta, p) e^{-i\omega t}] + f_F(p)$, where $p_x = p\cos\theta$, $p_y = p\sin\theta$, $|\delta f| \ll f_F$. Linearization of Eq. (6) gives

$$-i\omega\delta f + \frac{\partial W}{p\partial p}\frac{eH_z}{c}\frac{\partial \delta f}{\partial \theta} - e(\tilde{E}_x\cos\theta + \tilde{E}_y\sin\theta)\frac{\partial f_F}{\partial p} = 0.$$

This equation has an exact solution

$$\delta f = \frac{e}{\omega^2 - \left(\frac{\partial W}{p\partial p}\frac{eH_z}{c}\right)^2}\frac{\partial f_F}{\partial p}\left[\tilde{E}_x\left(i\omega\cos\theta - \frac{\partial W}{p\partial p}\frac{eH_z}{c}\sin\theta\right) + \tilde{E}_y\left(i\omega\sin\theta + \frac{\partial W}{p\partial p}\frac{eH_z}{c}\cos\theta\right)\right]. \tag{7}$$

The surface current is determined by

$$j_x = -eg\,\mathrm{Re}\left(e^{-i\omega t}\int \frac{\partial W}{\partial p}\cos\theta\delta f\, d^2p\right),$$
$$j_y = -eg\,\mathrm{Re}\left(e^{-i\omega t}\int \frac{\partial W}{\partial p}\sin\theta\delta f\, d^2p\right).$$

Substituting Eq. (7) in these equations and keeping only the terms linear with respect to the magnetic field we obtain the following expressions for the elements of the conductivity tensor σ_{ij}:

$$\sigma_{xx} = \sigma_{yy} = \sigma = -i\frac{g\pi e^2}{\omega}\int_0^\infty \frac{\partial W}{\partial p}\frac{\partial f_F}{\partial p}p\,dp,$$
$$\sigma_{xy} = -\sigma_{yx} = -\frac{e^3 g\pi H_z}{\omega^2 c}\int_0^\infty \left(\frac{\partial W}{\partial p}\right)^2\frac{\partial f_F}{\partial p}dp. \tag{8}$$

Using Eqs. (2) and (8), and the relationship between the complex conductivity and complex susceptibility $\chi_{ij} = \frac{i\sigma_{ij}}{\omega}$, we arrive at

$$m_z^{(0)} = -\frac{g\pi e^3}{2c\omega^3}\int_0^\infty \left(\frac{\partial W}{\partial p}\right)^2\frac{\partial f_F}{\partial p}dp \times \mathrm{Re}(i\tilde{E}_y\tilde{E}_x^*), \tag{9}$$

where the superscript (0) indicates the transparent medium approximation used to derive the Pitaevskii equation (1).

Since the effect is strongest when the electrons are strongly degenerate, we consider a zero-temperature 2D Fermi distribution as an unperturbed electron distribution

$$f_F(p) = \frac{1}{(2\pi\hbar)^2}\Theta(p_F - p), \tag{10}$$

where $\Theta(x)$ is the Heaviside step function. In this case, the integrals are easily calculated to give

$$\sigma_{xx} = \sigma_{yy} = \sigma = i\frac{ge^2 p_F}{4\pi\hbar^2\omega}\left(\frac{\partial W}{\partial p}\right)_{p=p_F},$$
$$\sigma_{xy} = -\sigma_{yx} = \frac{ge^3 H_z}{4\pi c\hbar^2\omega^2}\left(\frac{\partial W}{\partial p}\right)^2_{p=p_F}. \tag{11}$$

In particular, for graphene with linear dispersion ($g = 4$, $\frac{\partial W}{\partial p} = v_F$) the last of Eqs. (11) yields

$$\sigma_{xy}^{(\mathrm{intra})} = \frac{e^3 v_F^2 H_z}{\pi c\hbar^2\omega^2}. \tag{12}$$

Here, we added the label (intra) to emphasize the fact that the quasiclassical calculation gives only the intraband conductivity. For the magnetic moment we obtain

$$m_z^{(0)} = \frac{ge^3}{8\pi c\hbar^2\omega^3}\left(\frac{\partial W}{\partial p}\right)^2_{p=p_F} \times \mathrm{Re}(i\tilde{E}_y\tilde{E}_x^*). \tag{13}$$

It follows from Eq. (13) that if the electron dispersion is quadratic, the magnetization is proportional to the surface

electron density $n_F = \frac{gp_F^2}{4\pi\hbar^2}$ and inversely proportional to the square of their effective mass. For a linear dispersion near the Dirac point as in Eq. (4) and degenerate electron distribution of Eq. (10) the magnetization does not depend on the Fermi momentum p_F, i.e., it does not depend on the carrier density. One can write the result in the same form for both cases by introducing an effective mass for electrons at the Fermi level in graphene: $m_{\text{eff}} = \frac{p_F}{v_F}$. One has to keep in mind that the limit of small $p_F \to 0$ is not allowed as it would violate not only the criterion of negligible contribution from interband transitions, but also the applicability of the method of small perturbations that we used when solving the kinetic equation. The latter condition has the form $p_F \gg \frac{eE_0}{\omega}$, where $E_0 = |\tilde{\mathbf{E}}|$, as follows from the solution for the strong-field nonlinear problem solved in Appendix B.

III. QUANTUM THEORY OF THE IFE IN GRAPHENE

The magnetic moment generated as a result of IFE is determined by the magnetic field dependence of the off-diagonal element of the conductivity tensor. To find this dependence within full quantum theory we use the Kubo-Greenwood formula [51]

$$\sigma_{xy} = -\sigma_{yx} = i\hbar g \sum_{\alpha\beta} \left(\frac{f_\alpha - f_\beta}{E_\beta - E_\alpha}\right) \frac{\langle\alpha|\hat{j}_x|\beta\rangle\langle\beta|\hat{j}_y|\alpha\rangle}{\hbar(\omega + \frac{i}{\tau}) - (E_\beta - E_\alpha)}, \tag{14}$$

where $|\alpha\rangle$ are basis 2D surface states normalized by unit area $L_x \times L_y = 1$, E_α and f_α are the energy and population of state $|\alpha\rangle$, $\hat{j}_{x,y} = -ev_F\hat{\sigma}_{x,y}$ are Cartesian components of the current density operator [50], $g = 4$ is the degeneracy factor, τ is the relaxation time.

To determine the distribution function of carriers in a magnetic field oriented along the z axis, we extend the momentum operator in the Hamiltonian (3) in a standard way [52]: $\hat{\mathbf{p}} \Longrightarrow \hat{\mathbf{p}} - \mathbf{x}_0\frac{eH_z}{c}y$. The resulting electron eigenstates are [49]

$$|\alpha\rangle = |n,k\rangle = \frac{C_n}{\sqrt{L_y}} e^{-ik_y y} \begin{pmatrix} \text{sgn}(n) i^{|n|-1}\phi_{|n|-1} \\ i^{|n|}\phi_{|n|} \end{pmatrix}, \tag{15}$$

$$\phi_{|n|} = \frac{H_{|n|}\left(\frac{x-kl_c^2}{l_c}\right)}{\sqrt{2^{|n|}|n|!\sqrt{\pi}l_c}} \exp\left[-\frac{1}{2}\left(\frac{x-kl_c^2}{l_c}\right)^2\right], \tag{16}$$

where $H_n(\xi)$ is the Hermite polynomial, $l_c = \sqrt{\frac{\hbar c}{eH_z}}$ is the magnetic length, $n = 0, \pm1, \pm2, \ldots$ are principal numbers of the Landau levels, $C_0 = 1$, $C_{n\neq0} = \frac{1}{\sqrt{2}}$. The eigenenergy E_α depends only on the Landau level number $E_\alpha = E_n = \text{sgn}(n)\hbar\omega_c\sqrt{|n|}$, where $\omega_c = \frac{\sqrt{2}v_F}{l_c}$ is the cyclotron frequency.

Introducing the notations $|\alpha\rangle = |n,k\rangle$ and $|\beta\rangle = |m,k'\rangle$ and using Eqs. (15) and (16) we obtain the matrix elements of the components of the current density operator:

$$\langle\alpha|\hat{j}_{x,y}|\beta\rangle = -ev_F\langle\alpha|\hat{\sigma}_{x,y}|\beta\rangle = (j_{x,y})_{nm}\delta_{kk'}, \tag{17}$$

where

$$(j_x)_{nm} = -ev_F i^{|m|-|n|+1} C_n C_m [\text{sgn}(n)\delta(|n| - |m| - 1) - \text{sgn}(m)\delta(|n| - |m| + 1)], \tag{18}$$

$$(j_y)_{nm} = -ev_F i^{|m|-|n|} C_n C_m [\text{sgn}(m)\delta(|n| - |m| + 1) + \text{sgn}(n)\delta(|n| - |m| - 1)]. \tag{19}$$

The δ functions in Eqs. (18) and (19) determine the selection rules.

Performing the summation over k in Eq. (14) (see [52]) and using Eqs. (18) and (19), we arrive at the expression which contains the summation over the Landau level numbers:

$$\sigma_{xy} = -\frac{2\hbar}{\pi l_c^2} e^2 v_F^2 \sum_{mn} (C_n C_m)^2 \frac{f_n - f_m}{E_m - E_n} \frac{\delta(|n| - |m| - 1) - \delta(|n| - |m| + 1)}{\hbar(\omega + \frac{i}{\tau}) + (E_n - E_m)}, \tag{20}$$

where $1 \geqslant f_n \geqslant 0$; the degeneracy of a given Landau level per unit area is $\frac{2\hbar}{\pi l_c^2}$ including both spin and valley degeneracy.

In the case of a complete electron-hole symmetry, i.e., $f_0 = \frac{1}{2}$, $f_{n>0} = 0$, $f_{n<0} = 1$, from Eq. (20) we obtain $\sigma_{xy} \equiv 0$ for any H_z (see also [44]). Now, consider an n-doped system. Let the number n_F correspond to the highest occupied Landau level just below the Fermi energy, i.e., $W_F \geqslant \hbar\omega_c\sqrt{n_F}$. Since we need the limit of small magnetic fields, we assume that $W_F \gg \hbar\omega_c$, which can be written as

$$p_F l_c \gg \hbar. \tag{21}$$

This means that $n_F \gg 1$.

A. Contribution of intraband transitions

In this case we set $n, m > 0$ in Eq. (20). Consider a narrow vicinity of the Fermi energy where $|n - n_F| \ll n_F$ and $|E_{n_F} - W_F| \ll W_F$. In the limit of large n the distance between neighboring Landau levels is

$$\Delta E = E_{n+1} - E_n = \hbar\omega_c(\sqrt{n+1} - \sqrt{n}) \approx \frac{1}{2}\frac{\hbar\omega_c}{\sqrt{n_F}} \tag{22}$$

or

$$\Delta E = \frac{\hbar^2 v_F^2}{l_c^2 W_F}. \tag{23}$$

Note that introducing the effective mass $m_{\text{eff}} = \frac{p_F}{v_F}$ we obtain a standard relation $\Delta E = \frac{\hbar eH_z}{cm_{\text{eff}}}$.

Taking into account that $f_{n+1} - f_n \neq 0$ only in the near vicinity of the Fermi energy, from Eq. (20) we can

get

$$\sigma_{xy}^{(\mathrm{intra})} = -\frac{\hbar}{2\pi l_c^2} e^2 v_F^2 \frac{1}{\Delta E}\left[\frac{1}{\hbar\left(\omega+\frac{i}{\tau}\right)-\Delta E} - \frac{1}{\hbar\left(\omega+\frac{i}{\tau}\right)+\Delta E}\right]\sum_{n>0}(f_{n+1}-f_n), \tag{24}$$

where $\sum_{n>0}(f_{n+1}-f_n) \Longrightarrow \int_0^\infty df = -1$. The result is

$$\sigma_{xy}^{(\mathrm{intra})} = \frac{1}{\pi\hbar^2 c}\frac{e^3 v_F^2 H_z}{\left(\omega+\frac{i}{\tau}\right)^2 - \left(\frac{eH_z v_F}{cp_F}\right)^2}. \tag{25}$$

The last expression coincides with the semiclassical result derived from the kinetic equation (6) for $\hat{Q}(f) = \frac{f_F - f}{\tau}$. In particular, when $\tau \to \infty$ and $H_z \to 0$ we obtain Eq. (12).

B. Contribution of interband transitions

In this case, the numbers n and m in Eq. (20) have different signs. Taking this into account, we can write the sum in Eq. (20) as

$$\sigma_{xy}^{(\mathrm{inter})} = \frac{-\hbar e^2 v_F^2}{2\pi l_c^2}\left[\sum_{n<0,m>0}\frac{f_n - f_m}{E_m + |E_n|}\frac{\delta(n+m+1)-\delta(n+m-1)}{\hbar(\omega+\frac{i}{\tau}) - (|E_n|+E_m)} - \sum_{n>0,m<0}\frac{f_n - f_m}{|E_m| + E_n}\frac{\delta(n+m-1)-\delta(n+m+1)}{\hbar(\omega+\frac{i}{\tau}) + (E_n+|E_m|)}\right]. \tag{26}$$

Since in an n-doped degenerate system $f_{n>n_F} = 0$, $f_{n\leqslant n_F} = 1$, Eq. (26) yields

$$\sigma_{xy}^{(\mathrm{inter})} = -\frac{\hbar e^2 v_F^2}{2\pi\hbar^2 l_c^2}\left(\sum_{-(n_F+2)}^{-\infty}\frac{1}{\frac{E_{-n-1}+|E_n|}{\hbar}\left[(\omega+\frac{i}{\tau}) - \frac{E_{-n-1}+|E_n|}{\hbar}\right]} - \sum_{-n_F}^{-\infty}\frac{1}{\frac{E_{-n+1}+|E_n|}{\hbar}\left[(\omega+\frac{i}{\tau}) - \frac{E_{-n+1}+|E_n|}{\hbar}\right]}\right.$$
$$\left. - \sum_{n_F+1}^{\infty}\frac{1}{\frac{|E_{-n+1}|+E_n}{\hbar}\left[(\omega+\frac{i}{\tau}) + \frac{|E_{-n+1}|+E_n}{\hbar}\right]} + \sum_{n_F+1}^{\infty}\frac{1}{\frac{|E_{-n-1}|+E_n}{\hbar}\left[(\omega+\frac{i}{\tau}) + \frac{|E_{-n-1}|+E_n}{\hbar}\right]}\right). \tag{27}$$

Since the energy spectrum is symmetric, $|E_{-|n|}| = E_{|n|}$, we can regroup the terms on the right-hand side of Eq. (27) as

$$(\ldots) = -\frac{2}{\left(\omega+\frac{i}{\tau}\right)^2 - \left(\frac{E_{n_F+1}+t|E_{-n_F}|}{\hbar}\right)^2} - \sum_{n_F+2}^{\infty}\frac{2}{\left(\omega+\frac{i}{\tau}\right)^2 - \left(\frac{|E_{-n+1}|+E_n}{\hbar}\right)^2} + \sum_{n_F+1}^{\infty}\frac{2}{\left(\omega+\frac{i}{\tau}\right)^2 - \left(\frac{|E_{-n-1}|+E_n}{\hbar}\right)^2}.$$

It is easy to see that the sums on the right-hand side of the last equation cancel each other, leaving only the first term which is the contribution of the transition $-n_F \Longrightarrow n_F + 1$ (see Fig. 2). Taking into account that $\frac{E_{n_F+1}+|E_{-n_F}|}{\hbar} \approx \frac{2W_F}{\hbar}$ when the inequality Eq. (21) is satisfied, we obtain

$$\sigma_{xy}^{(\mathrm{inter})} = \frac{1}{\pi\hbar^2 c}\frac{e^3 v_F^2 H_z}{\left(\omega+\frac{i}{\tau}\right)^2 - \left(\frac{2W_F}{\hbar}\right)^2}. \tag{28}$$

Note that the expressions for the optical conductivity of graphene in a magnetic field were obtained in [53] where the direct Faraday effect was investigated.

In the absence of dissipation, the magnitude of the magnetic moment is determined by Eq. (2), which gives

$$m_z^{(0)} = \frac{1}{2\omega}\left[\frac{\partial\left(\sigma_{xy}^{(\mathrm{intra})} + \sigma_{xy}^{(\mathrm{inter})}\right)}{\partial H_z}\right]_{\tau\to\infty, H_z\to 0}\mathrm{Re}(i\tilde{E}_y\tilde{E}_x^*). \tag{29}$$

Using Eqs. (25) and (28) we finally arrive at

$$m_z^{(0)} = \frac{e^3 v_F^2}{2\pi c\hbar^2\omega^3}\frac{\left(\frac{2W_F}{\hbar}\right)^2 - 2\omega^2}{\left(\frac{2W_F}{\hbar}\right)^2 - \omega^2}\mathrm{Re}(i\tilde{E}_y\tilde{E}_x^*). \tag{30}$$

The frequency dependence of the magnetization is shown in Fig. 3. The incident light intensity was assumed to be 10 kW/cm^2, which is much less than the saturation intensity, so that the contribution of photoexcited carriers can be

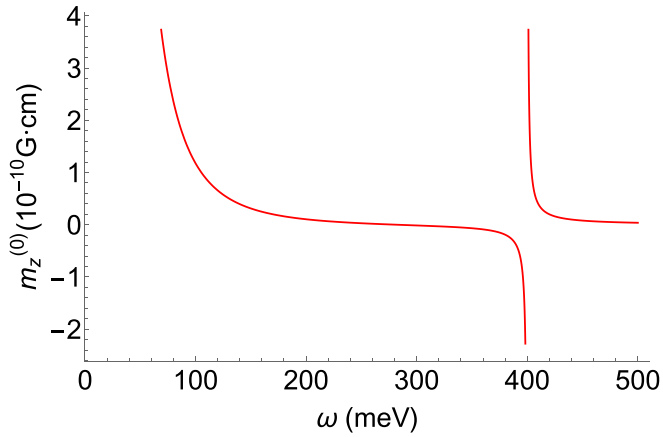

FIG. 3. Frequency dependence of the magnetization in Eq. (30) induced by a circularly polarized optical field of intensity 10 kW/cm^2. The Fermi energy $W_F = 0.2$ eV.

neglected. The magnitude of magnetization increases with decreasing frequency as $1/\omega^3$ when $\hbar\omega \ll W_F$ and the effect is dominated by intraband transitions. The magnetization changes sign twice: at $\hbar\omega = \sqrt{2}W_F$ and $\hbar\omega = 2W_F$. There is also a resonance at the interband transition edge $\hbar\omega = 2W_F$ where the magnitude of magnetization diverges. The divergence is an artifact of the dissipationless approximation which was used to relate magnetization to the off-diagonal susceptibility elements in Eq. (2). Obviously, relaxation processes cannot be neglected near resonance. Therefore, the validity of Eq. (30) in the resonance region is limited by $|\omega - 2W_F/\hbar| > \tau_{\text{inter}}^{-1}$, where τ_{inter} is the interband relaxation time. It is interesting that taking relaxation processes into account in the calculation of magnetization is not equivalent to using the complex susceptibility in Eq. (2) and taking the real part of the resulting expression. We will illustrate it in the next section within quasiclassical derivation.

As is clear from Fig. 3 and Eqs. (25), (28), and (30), when Eq. (5) is satisfied the interband transitions give only a small contribution to the IFE. In the analysis of the IFE in dissipative systems below, we will therefore neglect interband transitions.

IV. IFE IN A DISSIPATIVE SYSTEM: A QUASICLASSICAL THEORY

Here, we calculate the photogenerated magnetic moment per unit area without any assumptions of a dissipationless system. Therefore, we cannot use the Pitaevskii formula (1). Instead, we sum over magnetic moments of individual electrons undergoing induced motion in the optical field. First, we introduce surface polarization $\mathbf{P}$ and relate it with the surface current $\mathbf{j}$ in a standard way $\dot{\mathbf{P}} = \mathbf{j}$. Next, we represent polarization as $\mathbf{P} = -en_F\mathbf{R}$, where the vector $\mathbf{R}$ has a meaning of an average displacement of carriers and n_F is the surface density of a degenerate 2D electron gas. The magnetic moment per unit area is $\mathbf{m} = -n_F \times \frac{e}{2c}\langle \mathbf{R} \times \dot{\mathbf{R}} \rangle$, where the angular brackets mean averaging over the optical period $\frac{2\pi}{\omega}$. This expression is convenient to write as

$$\mathbf{m} = \mathbf{z}_0 m_z = -\frac{1}{2cen_F}\langle \mathbf{P} \times \mathbf{j} \rangle. \tag{31}$$

Substituting

$$\mathbf{j} = \text{Re}(\sigma(\omega)\tilde{\mathbf{E}}e^{-i\omega t}), \quad \mathbf{P} = \text{Re}\left(\frac{i}{\omega}\sigma(\omega)\tilde{\mathbf{E}}e^{-i\omega t}\right) \tag{32}$$

into Eq. (31), we obtain

$$m_z = \frac{|\sigma(\omega)|^2}{2ce\omega n_F}\text{Re}(i\tilde{E}_y\tilde{E}_x^*), \tag{33}$$

where $\sigma = \sigma_{xx} = \sigma_{yy}$; see Eq. (8). For a classical plasma, Eq. (33) was derived in [7].

To connect with the dissipationless limit in Eq. (2) we note that the elements of the conductivity tensor given by Eqs. (11) in a dissipationless system for any electron dispersion are related as

$$\frac{1}{ecn_F}\frac{i}{\omega}|\sigma|^2 = \left(\frac{i}{\omega}\frac{\partial\sigma_{xy}}{\partial H_z}\right)_{H_z\to 0} = \left(\frac{\partial\chi_{xy}}{\partial H_z}\right)_{H_z\to 0}. \tag{34}$$

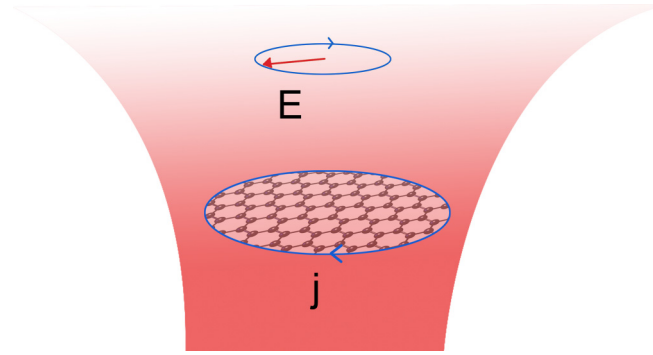

FIG. 4. A sketch of an edge photocurrent in a finite-size sample generated by an incident circularly polarized beam.

Substituting this into Eq. (33), we obtain the expression for magnetization which coincides with the phenomenological formula of Eq. (2).

Therefore, an approach based on Eqs. (31) and (32), which uses the conductivity $\sigma(\omega)$ calculated within a suitable microscopic model, leads to a correct result. Note that this approach is not based on dissipationless approximation. An advantage of an approach based on Eq. (31) is that there is no need to calculate the dielectric susceptibility tensor in the limit of a linear dependence on the external magnetic field $\mathbf{H}$. It is enough to calculate linear conductivity without an external magnetic field. In order to include dissipation, we use Eq. (6), assuming $\mathbf{H} = \mathbf{0}$ from the very beginning and adopting the simplest approximation for the relaxation operator: $\hat{Q}(f) = \frac{f_F - f}{\tau}$, where τ is the relaxation time. This is equivalent to the substitution $\omega \to \omega + \frac{i}{\tau}$ in the dissipationless formula for the conductivity. Then, Eq. (33) gives

$$m_z = m_z^{(0)}\frac{\omega^2}{\omega^2 + \tau^{-2}}, \tag{35}$$

where $m_z^{(0)}$ is the magnetization of a dissipationless system [see Eq. (13)]. One can see that Eq. (35) is not equivalent to using the complex susceptibility in Eq. (2) and taking the real part of the resulting expression.

At low frequencies, the finite size of a sample starts affecting the result; see Appendix A. The expression for the magnetic moment which is valid beyond the linearized theory is derived in Appendix B.

V. MAGNETIZATION CURRENT AND FINITE-SIZE EFFECTS

The magnetization current density generated in a 2D system as a result of IFE is given by $\mathbf{j} = c(\mathbf{x}_0\frac{\partial m_z}{\partial y} - \mathbf{y}_0\frac{\partial m_z}{\partial x})$. This equation yields a simple expression for the photocurrent around the boundary of a light beam or along the edge of an illuminated sample:

$$\mathbf{I} = c[\mathbf{n}_0 \times \mathbf{z}_0]m_z, \tag{36}$$

where $\mathbf{n}_0$ is a unit vector in the monolayer plane which is directed outside from the illuminated area perpendicularly to the boundary (see Fig. 4).

In a dissipative system, a simple expression (36) may be used with certain reservations. For example, the

magnetization current far from the sample edges can be affected by the viscosity of an electron fluid [54] whereas edge photocurrent can be affected by interaction of carriers with a sample boundary. (These effects can be responsible for various ways of detecting a constant current along the edge that are not related to IFE.) In fact, Eq. (36) corresponds to a mirror reflection of carriers from the boundary. Indeed, consider the edge $x = 0$ of a graphene sample, assuming that graphene extends to $x > 0$. The field component $E_x = \mathrm{Re}(\tilde{E}_x e^{-i\omega t})$ excites oscillations of carrier density in a boundary layer near the edge: $\delta n(x) = \mathrm{Re}(\delta\tilde{n}(x)e^{-i\omega t})$. Oscillations of an uncompensated charge $\delta\rho = -e\delta n$ should obey the continuity equation, which gives

$$i\omega e\int_0^\infty \delta\tilde{n}(x)dx = \sigma(\omega)\tilde{E}_x, \tag{37}$$

where the conductivity $\sigma(\omega)$ corresponds to the region where there is no uncompensated charge. Although the integration here should be formally extended to $x \to \infty$, in practice it is localized within a certain boundary layer much smaller than the sample dimensions.

The field component $E_y = \mathrm{Re}(\tilde{E}_y e^{-i\omega t})$ gives rise to the oscillations of carrier velocity along the edge. We can prove that for the elastic reflection of electrons from the boundary the average (hydrodynamic) velocity of electrons along the boundary (along y) is conserved up to cubic terms with respect to the field amplitude. Indeed, let us write the particle momentum as $\mathbf{p} = \mathbf{P} + \tilde{\mathbf{p}}(t)$, where $\mathbf{P}$ is its value averaged over time and $\tilde{\mathbf{p}} = \frac{e}{\omega}\mathrm{Re}(i^{-1}\tilde{\mathbf{E}}e^{-i\omega t})$ is an oscillating component. The velocity $\mathbf{v} = v_F\frac{\mathbf{p}}{|\mathbf{p}|}$ in the linear approximation with respect to the field $\mathbf{E}$ is given by $\tilde{\mathbf{v}} \approx v_F\left(\frac{\tilde{\mathbf{p}}}{|\mathbf{P}|} - \frac{\mathbf{P}(\mathbf{P}\cdot\tilde{\mathbf{p}})}{|\mathbf{P}|^3}\right)$, which gives

$$\tilde{v}_y = v_F\left(\tilde{p}_y\frac{P_x^2}{\left(P_x^2+P_y^2\right)^{\frac{3}{2}}} - \tilde{p}_x\frac{P_yP_x}{\left(P_x^2+P_y^2\right)^{\frac{3}{2}}}\right). \tag{38}$$

If the particle distribution is symmetric with respect to P_y, the ensemble-averaged velocity obtained from Eq. (38) is

$$\langle v_y\rangle = V_y = v_F\tilde{p}_y\frac{\left\langle P_x^2\right\rangle}{\left(P_x^2+P_y^2\right)^{\frac{3}{2}}}. \tag{39}$$

For elastic reflection, the momentum components P_y and $\tilde{p}_y$ are conserved separately whereas the magnitude of P_x^2 changes upon reflection. If P_{x1} and P_{x2} are the values before and after the reflection, then $P_{x2} = -[P_{x1} + 2\tilde{p}_x(t^*)]$, where t^* is the moment when the particle hits the edge. If the phases ωt^* are uniformly distributed, this effect contributes with the terms of the order of $|\tilde{E}_x|^2$, which leads to corrections cubic with respect to the field amplitude in Eq. (39). Neglecting these terms and also any effects of viscosity in the transition layer we obtain $V_y = \mathrm{Re}(\tilde{V}_y e^{-i\omega t})$, where $\tilde{V}_y = $ const. The result is

$$\tilde{V}_y = \tilde{V}_y(\infty) = \frac{\sigma(\omega)E_y}{-en_F}. \tag{40}$$

Now, we can calculate the constant (time-averaged) nonlinear edge photocurrent as

$$I_y = -\frac{e}{2}\mathrm{Re}\int_0^\infty \tilde{V}_y\delta\tilde{n}^*(x)dx. \tag{41}$$

Substituting here Eqs. (37) and (40) yields

$$I_y = \frac{1}{2en_F}\mathrm{Re}\frac{i}{\omega}|\sigma(\omega)|^2\tilde{E}_y\tilde{E}_x^*. \tag{42}$$

This result is exactly the same as the substitution of Eq. (33) into Eq. (36).

In the case of a very strong dissipation, when carriers are thermalized near the edge, one calculates the edge current using the approach described in [24]. This method relates the perturbation of carrier density with the perturbation of the chemical potential in the Fermi distribution. Applying this approach to a 2D system with linear electron dispersion gives the result which differs from Eq. (42) by a factor of $\frac{1}{2}$, whereas in a 3D with linear dispersion system the difference is a factor of $\frac{2}{3}$. In materials with a constant effective mass, the result is the same as Eq. (42). Note that in graphene and in typical semiconductors the thermalization time for carriers in a given band is longer than their scattering time by at least one order of magnitude; see, e.g., [33] and references therein. For a model with diffuse scattering at the boundary [45], the expression in Eq. (42) gives only an order-of-magnitude estimate.

VI. IFE IN WEYL SEMIMETALS

We consider the simplest model of a Dirac or Weyl type I semimetal (hereafter WSM) valid only at low enough frequencies in the near vicinity of a Weyl point, which is basically a 3D generalization of Eqs. (3) and (4), in which $\hat{\mathbf{p}}$ is a 3D momentum operator, $\hat{\boldsymbol{\sigma}} = \mathbf{x}_0\hat{\sigma}_x + \mathbf{y}_0\hat{\sigma}_y + \mathbf{z}_0\hat{\sigma}_z$ is a 3D vector of Pauli matrices, $(\mathbf{x}_0, \mathbf{y}_0, \mathbf{z}_0)$ are unit vectors along the coordinate axes, and

$$W(p) = sv_F\sqrt{p_x^2+p_y^2+p_z^2}. \tag{43}$$

Here, the number of Weyl nodes only adds to the degeneracy of electron states and the optical anisotropy and gyrotropy effects related to the finite separation of Weyl nodes [55] are neglected. The volume conductivity can be derived from a single-band kinetic equation if the radiation frequency ω, Fermi energy $v_F p_F$, and the distance b between Weyl nodes in k space are related by [55]

$$\hbar\omega \ll v_F p_F \ll \hbar v_F b.$$

For an unperturbed Fermi distribution in the conduction band,

$$f_F(p) = \frac{1}{(2\pi\hbar)^3}\Theta(p_F - p), \tag{44}$$

the conductivity has a Drude-type form [55]

$$\sigma = i\frac{e^2n_F}{\omega + \frac{i}{\tau}}\times\frac{v_F}{p_F}, \tag{45}$$

where $n_F = \frac{gp_F^3}{6\pi^2\hbar^3}$ is a volume density of electrons corresponding to the Fermi distribution (44); the degeneracy g takes into account the contribution of all Weyl nodes, including those with opposite chiralities.

First consider the collisionless limit. We can again use Eq. (6), taking $\hat{Q}(f) = 0$ and $\mathbf{E}\perp\mathbf{H}\parallel\mathbf{z}_0$. For a 3D system, the solution to Eq. (6) can be sought as $f = \mathrm{Re}[\delta f(\theta,\phi,p)e^{-i\omega t}] + f_F(p)$, where $p_x = p\cos\theta\sin\phi$,

$p_y = p\sin\theta\sin\phi$, $p_z = p\cos\phi$; $|\delta f| \ll f_F$. Linearizing Eq. (6) and taking into account electron dispersion Eq. (43) gives

$$-i\omega\delta f + \frac{v_F}{p}\frac{eH_z}{c}\frac{\partial\delta f}{\partial\theta} - e(\tilde{E}_x\cos\theta + \tilde{E}_y\sin\theta)\sin\phi\frac{\partial f_F}{\partial p} = 0. \quad (46)$$

Equation (46) has the following solution:

$$\delta f = \frac{e}{\omega^2 - \left(\frac{v_F}{p}\frac{eH_z}{c}\right)^2}\frac{\partial f_F}{\partial p}\sin\phi\left[\tilde{E}_x\left(i\omega\cos\theta - \frac{v_F}{p}\frac{eH_z}{c}\sin\theta\right) + \tilde{E}_y\left(i\omega\sin\theta + \frac{v_F}{p}\frac{eH_z}{c}\cos\theta\right)\right]. \quad (47)$$

The corresponding current density is

$$j_x = -egv_F\mathrm{Re}\left(e^{-i\omega t}\int\sin\phi\cos\theta\delta f\, d^3p\right),$$
$$j_y = -egv_F\mathrm{Re}\left(e^{-i\omega t}\int\sin\phi\sin\theta\delta f\, d^3p\right). \quad (48)$$

From Eqs. (47) and (48) one can obtain the components of the conductivity tensor, keeping only the terms linear with respect to the magnetic field:

$$\sigma_{xx} = \sigma_{yy} = \sigma = \frac{4\pi ie^2gv_F}{3\omega}\int_0^\infty 2f_F p\, dp,$$
$$\sigma_{xy} = -\sigma_{yx} = \frac{4\pi e^3gH_zv_F^2}{3\omega^2c}\int_0^\infty f_F\, dp. \quad (49)$$

This gives the desired components of the dielectric permittivity tensor $\varepsilon_{ij} = \delta_{ij} + 4\pi\frac{i\sigma_{ij}}{\omega}$, and finally the magnetic moment calculated using Eq. (1):

$$m_z^{(0)} = \frac{1}{8\pi}\mathrm{Re}\left[\left(\frac{\partial\varepsilon_{xy}^{(\mathrm{intra})}}{\partial H_z}\right)_{H_z\to0}\tilde{E}_y\tilde{E}_x^*\right] = \frac{2\pi e^3gH_zv_F^2}{3\omega^3c}\int_0^\infty f_F\, dp\times\mathrm{Re}(i\tilde{E}_y\tilde{E}_x^*), \quad (50)$$

where the superscript (0) is again to indicate an approximation of a transparent medium.

For a degenerate electron distribution in the zero-temperature limit (44) we have

$$\sigma_{xx} = \sigma_{yy} = \sigma = i\frac{e^2gp_F^2v_F}{6\hbar^3\pi^2\omega},$$
$$\sigma_{xy} = -\sigma_{yx} = \frac{e^3gH_zp_Fv_F^2}{6\hbar^3\pi^2\omega^2c}, \quad (51)$$

and

$$m_z^{(0)} = \frac{e^3gp_Fv_F^2}{12\hbar^3\pi^2\omega^3c}\mathrm{Re}(i\tilde{E}_y\tilde{E}_x^*). \quad (52)$$

As in the case of a 2D material, these components of the conductivity tensor coincide with those obtained for particles with a constant mass m_{eff}, if we express them through a particle density n_F and introduce the effective mass as $m_{\mathrm{eff}} = \frac{p_F}{v_F}$.

It is also easy to find out that Eqs. (49) satisfy the equations similar to those for 2D systems in Eq. (34):

$$\frac{1}{ecn_F}\frac{i}{\omega}|\sigma|^2 = \left(\frac{i}{\omega}\frac{\partial\sigma_{xy}}{\partial H_z}\right)_{H_z\to0} = \frac{1}{4\pi}\left(\frac{\partial\varepsilon_{xy}}{\partial H_z}\right)_{H_z\to0}. \quad (53)$$

When scattering and dissipation are taken into account, one can repeat the same derivation steps as above for a 2D system and arrive at the expression for the photogenerated magnetic moment in the form of Eq. (33), in which one should substitute the volume conductivity Eq. (45) and volume carrier density n_F.

VII. DISCUSSION

In order to compare the magnitude of the IFE in Dirac materials with that in conventional semiconductors, we note that for materials with conventional quadratic dispersion of carriers the induced magnetic moment per free carrier scales inversely proportional to their effective mass squared. As we already pointed out, the same dependence exists in both 2D and 3D Dirac materials if we denote $m_{\mathrm{eff}} = \frac{p_F}{v_F} = \frac{W_F}{v_F^2}$ as an effective mass. Assuming $v_F \approx c/300$, the ratio of the effective to free-electron mass is $\frac{m_{\mathrm{eff}}}{m_0} \simeq 2\times10^{-4}\frac{W_F}{1\ \mathrm{meV}}$. For example, when $W_F = 50$ meV, the effective mass is $0.01m_0$, which is one order of magnitude lower than in a typical semiconductor with a band gap of the order of 1 eV. Therefore, at low frequencies $\hbar\omega \ll W_F$, the IFE in Dirac materials can be stronger than in conventional semiconductors by a couple of orders of magnitude.

Let us estimate the magnetization obtained in the experiment [45], where the excitation of edge photocurrent in graphene was investigated. They used an NH_3 laser with 10 kW power and minimum frequency of 1.1 THz. For a 1-mm radius of a laser focus and Fermi energy of 0.2–0.3 eV the condition $p_F \gg \frac{eE_0}{\omega}$ is satisfied. Using the current dissipation time $\tau \sim 100$ fs (which corresponds to $\omega\tau \sim 1$), the magnetic moment of an illuminated spot is about $\sim10^{-7}$ G cm^3, and the photoinduced average magnetic moment per free carrier particle is of the order of 100 Bohr magnetons.

If the optical pumping creates the magnetic moment of 100 Bohr magnetons per carrier, the magnetic moment per unit area of graphene scales as $4\pi m_z \sim 10^{-5}(\frac{W_F}{100\ \mathrm{meV}})^2$ G cm. Similarly, the magnetic moment per unit volume in an illuminated volume of a Weyl semimetal sample scales roughly as $4\pi m_z \sim 2.2g(\frac{W_F}{100\ \mathrm{meV}})^3$ G, where g is degeneracy including the total number of Weyl nodes.

One possible application for the IFE is to provide all-optical modulation of the polarization of the probe light transmitted through (or reflected from) an area of the optical excitation. For example, a probe light passing along the z axis through the area of optically induced magnetization m_z experiences *direct* Faraday effect. The magnitude of the polarization rotation χ can be calculated using textbook Faraday effect formulas in which an external magnetic field B_z is replaced by $4\pi m_z$, where m_z is an optically induced magnetic moment per unit volume:

$$\chi(L) = \int_0^L \alpha\, dz, \quad (54)$$

where

$$\alpha = \frac{\omega}{2c}(n_O - n_X) \tag{55}$$

and $n_{O,X}$ are refractive indices of normal electromagnetic modes, i.e., ordinary and extraordinary modes. In the simplest case of a dielectric tensor with $\varepsilon_{xx} = \varepsilon_{yy}$ the normal modes are circularly polarized and

$$n_{O,X}^2 = \varepsilon_{xx} \pm |\varepsilon_{xy}|, \tag{56}$$

where $\varepsilon_{xx} = \varepsilon_{yy} = 1 + 4\pi i\sigma/\omega$. For small magnetic fields $\varepsilon_{xy} \propto B_z$, so Eqs. (55) and (56) give

$$\alpha \approx \frac{\omega}{2c\sqrt{\varepsilon_{xx}}}|\varepsilon_{xy}| \approx \frac{\omega}{2c\sqrt{\varepsilon_{xx}}}\left|\left(\frac{\partial\varepsilon_{xy}}{\partial B_z}\right)_{B_z\to 0} B_z\right|. \tag{57}$$

Note that for the material with no intrinsic magnetic order and for linear dependence of the off-diagonal component of the dielectric tensor on the magnetic field, we can replace the magnetic field H_z with the magnetic induction B_z in all expressions in this paper. Then, taking into account that

$$m_z = \frac{1}{8\pi}\left(\frac{\partial\varepsilon_{xy}}{\partial B_z}\right)_{B_z\to 0}|E|^2,$$

we obtain

$$\alpha = \frac{\omega}{4c}\frac{1}{\sqrt{1+4\pi i\sigma/\omega}}\left(\frac{\partial\varepsilon_{xy}}{\partial B_z}\right)^2_{B_z\to 0}|E|^2, \tag{58}$$

where

$$\sigma = i\frac{e^2 g v_F p_F^2}{6\hbar^3\pi^2\omega},$$

$$\left|\frac{\partial\varepsilon_{xy}}{\partial B_z}\right|_{B_z\to 0} = \frac{4\pi}{\omega}\left|\frac{\partial\sigma_{xy}}{\partial B_z}\right|_{B_z\to 0} = \frac{2e^3 g v_F^2 p_F}{3\hbar^3\pi\omega^3 c}.$$

For a specific example, consider an incident optical pump with the electric field of magnitude 10 kV/cm at frequency $\omega/2\pi = 1$ THz. For the Fermi energy of 100 meV in a WSM sample, the Faraday rotation parameter $\alpha \approx 6.6g^{3/2}$ rad/cm, which is already interesting for applications. The modulation magnitude could be further enhanced by integration of a Dirac material with a suitable plasmonic structure which supports highly localized plasmon modes. For example, in [56] a strong enhancement of Faraday rotation was predicted for a graphene sheet encapsulated in a 2D metallic grating.

VIII. CONCLUSIONS

In conclusion, we investigated the inverse Faraday effect in materials with massless Dirac fermions, both in two dimensions such as graphene and surface states in topological insulators, and in three dimensions such as Dirac and Weyl semimetals. Both semiclassical and quantum theories were presented. The dissipation, finite size, and strong field effects were analyzed in the quasiclassical approximation. We found that the magnitude of the IFE can be significantly enhanced in Dirac materials as compared to conventional semiconductors. This makes Dirac materials promising for the optical control of magnetization, all-optical modulation, and optical isolation in compact optoelectronic devices.

ACKNOWLEDGMENTS

This work has been supported in part by the Air Force Office for Scientific Research through Grant No. FA9550-17-1-0341 and by NSF Award No. 1936276. M.T. acknowledges the support from RFBR Grant No. 18-29-19091mk. I.O. acknowledges the support from Federal Research Center Institute of Applied Physics of the Russian Academy of Sciences (Project No. 0035-2019-004). I.D.T., I.A.S., and V.I.P. acknowledge the support by RFBR Grants No. 18-02-00390 and No. 19-31-51019 and the Russian State Contract No. 0035-2019-0021.

APPENDIX A: FINITE SAMPLE EFFECTS AND THE DEPOLARIZATION FIELD

Consider a sample shaped as a thin disk of radius R in the (x, y) plane and introduce polar coordinates r and φ on the disk. Consider a circularly polarized optical field incident on a disk, with electric field vector components

$$E_x = E_0\cos(\omega t), \quad E_y = -E_0\sin(\omega t), \tag{A1}$$

where $\omega > 0$ corresponds to the clockwise rotation of the vector $\mathbf{E}$ and $\omega < 0$ to the counterclockwise rotation. The rotating field excites a rotating current in the disk:

$$j_x = j_0\cos(\omega t + \phi), \quad j_y = -j_0\sin(\omega t + \phi), \tag{A2}$$

where the phase shift ϕ is determined by dissipative processes in the sample. The current given by Eqs. (A2) corresponds to the rotating electric polarization:

$$P_x = P_0\sin(\omega t + \phi), \quad P_y = P_0\cos(\omega t + \phi), \tag{A3}$$

where $P_0 = \frac{j_0}{\omega}$, i.e., $\dot{P}_x = j_x$, $\dot{P}_y = j_y$.

The current excitation by a time-dependent external field in a finite sample leads to an uncompensated time-dependent charge at a certain distance l from the disk edge. The magnitude of the charge depends on the specific mechanism of interaction of carriers with a boundary. Strictly speaking, both the current and the electric polarization are described by Eqs. (A2) and (A3) only at a certain distance $\rho \geqslant l$ from the disk edge. Since we do not want to get into the details of the carrier-boundary interaction, we will assume that the width of the boundary layer is much smaller than the disk radius: $l \ll R$.

Let us denote an uncompensated charge per unit length along the disk edge as $\delta\rho(t, \varphi)$. It can be expressed as $\delta\rho = P_r$, where P_r is the normal component of the polarization vector: $P_r = P_x\cos\varphi + P_y\sin\varphi$. The edge charge leads to generation of the depolarization field $\mathbf{E}_p$ [1]. For a uniform external field given by Eq. (A1), we can use the solution of a corresponding electrostatic problem in [1]. If we approximate a thin disk with an ellipsoid of rotation with semiminor axis $a \ll R$, we get

$$\mathbf{E}_p = -\frac{\pi^2}{2R}\mathbf{P},$$

where $\mathbf{P}$ is a 2D density of the dipole moment. Taking into account the effect of the depolarization field and Eqs. (A1)–(A3), we obtain

$$\sigma\left[E_0 - i\frac{\pi^2}{2R\omega}j_0 e^{-i\phi}\right] = j_0 e^{-i\phi}, \quad j_0 e^{-i\phi} = E_0\frac{\sigma}{1 + i\sigma\frac{\pi^2}{2R\omega}},$$

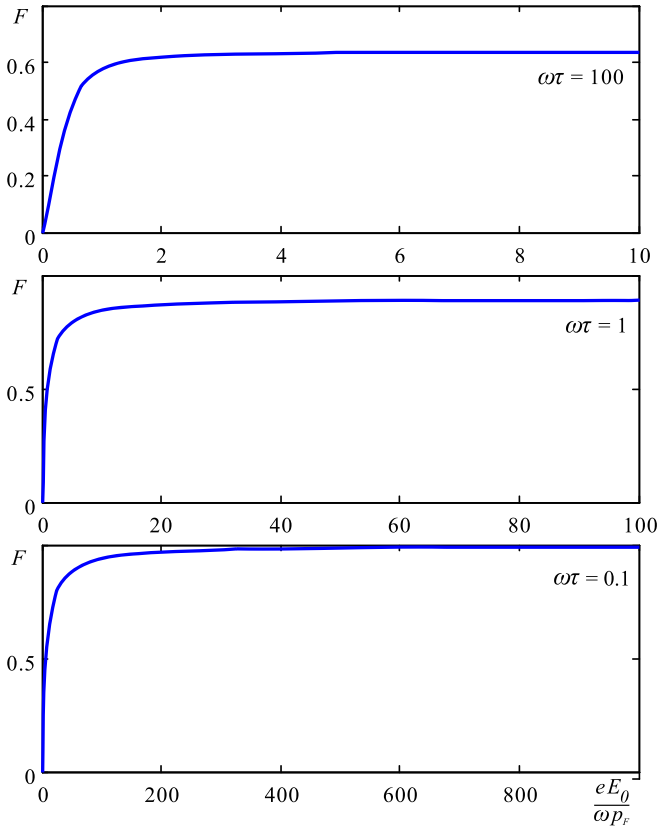

FIG. 5. $F(\frac{eE_0}{\omega p_F}, \omega\tau)$ as a function of the parameter $\frac{eE_0}{\omega p_F}$ at different $\omega\tau$.

where σ is a 2D conductivity of the layer including relaxation processes. Using Eq. (31) for the magnetic moment, we arrive at the expression which generalizes Eq. (35):

$$m_z = m_z^{(0)} \frac{\omega^4}{\left(\omega^2 - \omega_p^2\right)^2 + \omega^2\tau^{-2}}, \tag{A4}$$

where $m_z^{(0)}$ is the magnitude of the magnetic moment generated by a circularly polarized field without including dissipation and depolarization effects, $\omega_p = \sqrt{\frac{\pi g e^2 p_F v_F}{8\hbar^2 R}}$, where $\frac{\partial W}{\partial p} = v_F$. The resonant frequency ω_p in Eq. (A4) coincides up to a numerical factor with the frequency of 2D plasmons in graphene at wavelength $2R$ (see, e.g., [57]). In the limit $R \to \infty$, Eq. (A4) gives the result for an infinite medium.

APPENDIX B: IFE IN GRAPHENE BEYOND SMALL PERTURBATION

Here, we consider an incident radiation of an arbitrarily strong intensity and go beyond the linear approximation. Let us again assume a circularly polarized field given by Eq. (A1). The kinetic equation (6) with $\mathbf{H} = \mathbf{0}$ and relaxation operator $\hat{Q}(f) = \frac{f_F - f}{\tau}$ takes the form

$$\frac{\partial f(\mathbf{p},t)}{\partial t} - eE_0\cos(\omega t)\frac{\partial f(\mathbf{p},t)}{\partial p_x} + eE_0\sin(\omega t)\frac{\partial f(\mathbf{p},t)}{\partial p_y} = \frac{f_F(p) - f(\mathbf{p},t)}{\tau}. \tag{B1}$$

Its solution in quadratures can be found by the method of characteristics. At times $t \gg \tau$ for any initial conditions the solution approaches

$$f = e^{-\frac{t}{\tau}}\frac{1}{\tau}\int_0^t dt' e^{\frac{t'}{\tau}} f_F\left[p_x + \frac{eE_0}{\omega}(\sin\omega t - \sin\omega t'), p_y + \frac{eE_0}{\omega}(\cos\omega t - \cos\omega t')\right]. \tag{B2}$$

After cumbersome but fairly straightforward derivation, the surface current density $\mathbf{j} = -egv_F\int \frac{\mathbf{p}}{p} f\, d^2p$ can be found:

$$j_x = -en_F V_x(t), \quad j_y = -en_F V_y(t). \tag{B3}$$

Here, the functions $V_{x,y}(t)$ are given by

$$V_x(t) = \frac{v_F}{1 - e^{-\frac{2\pi}{|\omega|\tau}}}\int_0^{\frac{2\pi}{|\omega|\tau}} e^{-z}\Phi\left(\frac{eE_0}{\omega p_F}, \omega\tau z\right) \times \{[1 - \cos(\omega\tau z)]\sin(\omega t) + \sin(\omega\tau z)\cos(\omega t)\}dz, \tag{B4}$$

$$V_y(t) = \frac{v_F}{1 - e^{-\frac{2\pi}{|\omega|\tau}}}\int_0^{\frac{2\pi}{|\omega|\tau}} e^{-z}\Phi\left(\frac{eE_0}{\omega p_F}, \omega\tau z\right) \times \{[1 - \cos(\omega\tau z)]\cos(\omega t) + \sin(\omega\tau z)\sin(\omega t)\}dz, \tag{B5}$$

where

$$\Phi\left(\frac{eE_0}{\omega p_F}, \omega\tau z\right) = \left(\frac{2eE_0}{\pi\omega p_F}\right)\int_0^{\pi}\frac{\sin^2\alpha}{\sqrt{1 + 4\left(\frac{eE_0}{\omega p_F}\right)^2\sin^2\left(\frac{\omega\tau z}{2}\right) + 4\left|\frac{eE_0}{\omega p_F}\sin\left(\frac{\omega\tau z}{2}\right)\right|\cos\alpha}}d\alpha. \tag{B6}$$

It follows from (B3)–(B6) that the surface current density vector can be presented in the form of Eq. (A2), in which

$$j_0 = ev_F n_F F\left(\frac{eE_0}{\omega p_F}, \omega\tau\right),$$

$$F\left(\frac{eE_0}{\omega p_F}, \omega\tau\right) = \left(1 - e^{-\frac{2\pi}{|\omega|\tau}}\right)^{-1}\left(\left\{\int_0^{\frac{2\pi}{|\omega|\tau}} e^{-z}\Phi\left(\frac{eE_0}{\omega p_F}, \omega\tau z\right)[1 - \cos(\omega\tau z)]dz\right\}^2 + \left\{\int_0^{\frac{2\pi}{|\omega|\tau}} e^{-z}\Phi\left(\frac{eE_0}{\omega p_F}, \omega\tau z\right)\sin(\omega\tau z)dz\right\}^2\right)^{1/2}. \tag{B7}$$

The value of the phase shift ϕ does not matter in this case.

Figure 5 shows the dependence $F(\frac{eE_0}{\omega p_F}, \omega\tau)$ on the parameter $\frac{eE_0}{\omega p_F}$ at different $\omega\tau$. There is an obvious saturation effect at $\frac{eE_0}{\omega p_F} \gg 1$. The current defined by Eqs. (A2) and (B7) corresponds to the surface polarization given by Eq. (A3). Using the expression (31) for the magnetization, we arrive at

$$m_z = \frac{en_F v_F^2}{2c\omega} F^2\left(\frac{eE_0}{\omega p_F}, \omega\tau\right). \tag{B8}$$

For weak fields, when $\frac{eE_0}{\omega p_F} \ll 1$, we have the limit

$$\Phi\left(\frac{eE_0}{\omega p_F}, \omega\tau z\right) \cong \frac{eE_0}{\omega p_F}, \quad F\left(\frac{eE_0}{\omega p_F}, \omega\tau\right) \cong \frac{eE_0}{p_F\sqrt{\tau^{-2}+\omega^2}}.$$

In this case, Eq. (B8) is reduced to Eq. (35) for $\tilde{E}_y = -i\,\tilde{E}_x$, $\tilde{E}_x = E_0$. The expression in Eq. (B8) allows one to estimate the magnitude of the IFE for strong fields, when $\frac{eE_0}{\omega p_F} \geqslant 1$.

[1] L. D. Landau and E. M. Lifshitz, *Electrodynamics of Continuous Media* (Pergamon, Oxford, 1984).
[2] L. P. Pitaevskii, Zh. Eksp. Theor. Fiz. **39**, 1450 (1960 [Sov. Phys.–JETP **12**, 1008 (1961)].
[3] J. P. van der Ziel, P. S. Pershan, and L. D. Malstrom, Phys. Rev. Lett. **15**, 190 (1965).
[4] P. S. Pershan, Phys. Rev. **130**, 919 (1963).
[5] P. S. Pershan, J. P. van der Ziel, and L. D. Malstrom, Phys. Rev. **143**, 574 (1966).
[6] V. I. Karpman and A. G. Shagalov, J. Plasma Phys. **27**, 215 (1982).
[7] M. D. Tokman, Fiz. Plasmy **10**, 568 (1984) [Sov. J. Plasma Phys. **10**, 331 (1984)].
[8] Y. Horovitz, S. Eliezer, A. Ludmirsky, Z. Henis, E. Moshe, R. Shpitalnik, and B. Arad, Phys. Rev. Lett. **78**, 1707 (1997).
[9] Z. Najmudin, M. Tatarakis, A. Pukhov, E. L. Clark, R. J. Clarke, A. E. Dangor, J. Faure, V. Malka, D. Neely, M. I. K. Santala, and K. Krushelnick, Phys. Rev. Lett. **87**, 215004 (2001).
[10] N. Nasery, V. Yu. Bychenkov, and W. Rozmus, Phys. Plasmas **17**, 033107 (2010).
[11] R. Hertel, J. Magn. Magn. Mater. **303**, L1 (2006).
[12] R. Hertel and M. Fähnle, Phys. Rev. B **91**, 020411(R) (2015).
[13] I. D. Tokman, Phys. Lett. A **252**, 83 (1999).
[14] C. D. Stanciu, F. Hansteen, A. V. Kimel, A. Tsukamoto, A. Itoh, A. Kirilyuk, and Th. Rasing, Phys. Rev. Lett. **98**, 207401 (2007).
[15] K. Vahaplar, A. M. Kalashnikova, A. V. Kimel, S. Gerlach, D. Hinzke, U. Nowak, R. Chantrell, A. Tsukamoto, A. Itoh, A. Kirilyuk, and Th. Rasing, Phys. Rev. B **85**, 104402 (2012).
[16] F. Hansteen, A. Kimel, A. Kirilyuk, and Th. Rasing, Phys. Rev. B **73**, 014421 (2006).
[17] A. H. M. Reid, A. V. Kimel, A. Kirilyuk, J. F. Gregg, and Th. Rasing, Phys. Rev. Lett. **105**, 107402 (2010).
[18] T. Makino, F. Liu, T. Yamasaki, Y. Kozuka, K. Ueno, A. Tsukazaki, T. Fukumura, Y. Kong, and M. Kavasaki, Phys. Rev. B **86**, 064403 (2012).
[19] Z. Jin, H. Ma, D. Li, G. Ma, M. Wang, and C. Zhao, J. Appl. Phys. **109**, 073109 (2011).
[20] T. Satoh, S.-J. Cho, R. Iida, T. Shimura, K. Kuroda, H. Ueda, Y. Ueda, B. A. Ivanov, F. Nori, and M. Fiebig, Phys. Rev. Lett. **105**, 077402 (2010).
[21] A. H. M. Reid, A. V. Kimel, A. Kirilyuk, J. F. Gregg, and Th. Rasing, Phys. Rev. B **81**, 104404 (2010).
[22] A. Kirilyuk, A. V. Kimel, and Th. Rasing, Rev. Mod. Phys. **82**, 2731 (2010).
[23] R. Iida, T. Satoh, T. Shimura, K. Kuroda, B. A. Ivanov, Y. Tokunaga, and Y. Tokura, Phys. Rev. B **84**, 064402 (2011).
[24] M. M. Glazov and S. D. Ganichev, Phys. Rep. **535**, 101 (2014).
[25] F. Bonaccorso, Z. Sun, T. Hasan, and A. C. Ferrari, Nat. Photonics **4**, 611 (2010).
[26] T. Otsuji, S. A. Boubanga Tombet, A. Satou, H. Fukidome, M. Suemitsu, E. Sano, V. Popov, M. Ryzhii, and V. Ryzhii, J. Phys. D: Appl. Phys. **45**, 303001 (2012).
[27] M. M. Glazov, JETP Lett. **93**, 366 (2011).
[28] S. A. Mikhailov, Phys. Rev. B **95**, 085432 (2017).
[29] X. Yao, M. Tokman, and A. Belyanin, Phys. Rev. Lett. **112**, 055501 (2014).
[30] M. Tokman, Y. Wang, I. Oladyshkin, A. R. Kutayiah, and A. Belyanin, Phys. Rev. B **93**, 235422 (2016).
[31] Y. Wang, M. Tokman, and A. Belyanin, Phys. Rev. B **94**, 195442 (2016).
[32] J. Cheng, L. N. Vermeulen, and J. E. Sipe, Sci. Rep. **7**, 43843 (2017).
[33] I. V. Oladyshkin, S. B. Bodrov, Yu. A. Sergeev, A. I. Korytin, M. D. Tokman, and A. N. Stepanov, Phys. Rev. B **96**, 155401 (2017).
[34] J. J. Dean and H. M. van Driel, Phys. Rev. B **82**, 125411 (2010).
[35] D. A. Smirnova, I. V. Shadrivov, A. E. Miroshnichenko, A. I. Smirnov, and Y. S. Kivshar, Phys. Rev. B **90**, 035412 (2014).
[36] S. A. Mikhailov, Phys. Rev. B **93**, 085403 (2016).
[37] J. L. Cheng, N. Vermeulen, and J. E. Sipe, New J. Phys. **16**, 053014 (2014); **18**, 029501 (2016).
[38] M. Tokman, S. B. Bodrov, Y. A. Sergeev, A. I. Korytin, I. Oladyshkin, Y. Wang, A. Belyanin, and A. N. Stepanov, Phys. Rev. B **99**, 155411 (2019).
[39] M. Tokman, X. Yao, and A. Belyanin, Phys. Rev. Lett. **110**, 077404 (2013).
[40] S. A. Mikhailov, Phys. Rev. B **79**, 241309(R) (2009).
[41] M. D. Tokman, M. A. Erukhimova, and A. Belyanin, JETP Lett. **100**, 390 (2014).
[42] X. Yao and M. Tokman, and A. Belyanin, Opt. Express **23**, 795 (2015).
[43] A. R. Kutayiah, M. Tokman, Y. Wang, and A. Belyanin, Phys. Rev. B **98**, 115410 (2018).
[44] Z. Long, Y. Wang, M. Erukhimova, M. Tokman, and A. Belyanin, Phys. Rev. Lett. **120**, 037403 (2018).
[45] J. Karch, C. Drexler, P. Olbrich, M. Fehrenbacher, M. Hirmer, M. M. Glazov, S. A. Tarasenko, E. L. Ivchenko, B. Birkner, J. Eroms, D. Weiss, R. Yakimova, S. Lara-Avila, S. Kubatkin, M. Ostler, T. Seyller, and S. D. Ganichev, Phys. Rev. Lett. **107**, 276601 (2011).
[46] M. Battiato, G. Barbalinardo, and P. M. Oppeneer, Phys. Rev. B **89**, 014413 (2014).

[47] V. L. Ginzburg, *Theoretical Physics and Astrophysics* (Pergamon, Oxford, 1979).
[48] Y. Zheng and T. Ando, Phys. Rev. B **65**, 245420 (2002).
[49] J. W. McClure, Phys. Rev. **104**, 666 (1956).
[50] M. I. Katsnelson, *Graphene: Carbon in Two Dimensions* (Cambridge University Press, New York, 2012).
[51] G. D. Mahan, *Many-Particle Physics*, Physics of Solids and Liquids, 3rd ed. (Springer, New York, 2000).
[52] L. D. Landau and E. M. Lifshits, *Quantum Mechanics: Nonrelativistic Theory*, 3rd ed. (Pergamon, Oxford, 1977).
[53] A. Ferreira, J. Viana-Gomes, Yu. V. Bludov, V. Pereira,, N. M. R. Peres, and A. H. Castro Neto, Phys. Rev. B **84**, 235410 (2011).
[54] L. Levitov and G. Falkovich, Nat. Phys. **12**, 672 (2016).
[55] Q. Chen, A. R. Kutayiah, I. Oladyshkin, M. Tokman, and A. Belyanin, Phys. Rev. B **99**, 075137 (2019).
[56] Yu. V. Bludov, M. I. Vasilevskiy, and N. M. R. Peres, Phys. Rev. B **97**, 045433 (2018).
[57] E. H. Hwang and S. Das Sarma, Phys. Rev. B **75**, 205418 (2007).